Iranian Journal of Numerical Analysis and Optimization
Vol. 8, No. 1, (2018), pp 41–61
DOI:10.22067/ijnao.v8i1.62683

WENO schemes for multidimensional nonlinear degenerate parabolic PDEs

R. Abedian*

Abstract

In this paper, a scheme is presented for approximating solutions of nonlinear degenerate parabolic equations which may contain discontinuous solutions. In the one-dimensional case, following the idea of the local discontinuous Galerkin method, first the degenerate parabolic equation is considered as a nonlinear system of first order equations, and then this system is solved using a fifth-order finite difference weighted essentially nonoscillatory (WENO) method for conservation laws. This is the first time that the minmod-limiter combined with weighted essentially nonoscillatory procedure has been applied to the degenerate parabolic equations. Also, it is necessary to mention that the new scheme has fifth-order accuracy in smooth regions and second-order accuracy near singularities. The accuracy, robustness, and high-resolution properties of the new scheme are demonstrated in a variety of multidimensional problems.

Keywords: WENO schemes; Finite difference scheme; Multidimensional nonlinear degenerate parabolic equation; Porous medium equation.

1 Introduction

This paper is concerned with multidimensional of nonlinear degenerate parabolic equations of the form

$$u_t = \Delta \mathbf{b}(u) + S(\mathbf{x}, t, u), \qquad \mathbf{x} = (x_1, \ldots, x_d) \in \Omega \text{ and } \ t \geq 0, \qquad (1)$$

satisfying the initial condition

*Corresponding author
Received 17 February 2017; revised 7 may 2017; accepted 12 July 2017
R. Abedian
School of Engineering Science, College of Engineering, University of Tehran, Iran. e-mail: rabedian@ut.ac.ir

$$u(\mathbf{x}, 0) = u_0(\mathbf{x}), \qquad \mathbf{x} \in \Omega, \tag{2}$$

and suitable boundary conditions. The condition $D_j(u) = b'_j(u) \geq 0$, $j = 1, \ldots, d$ is needed to make the equation formally parabolic. Whenever $D_j(u) = 0$, for some $u \in \mathbb{R}$, is said that the equation degenerates at that $u-$level, since it ceases to be strictly parabolic. For $b_j(u) = u^m$, $m > 1$, and $S(\mathbf{x}, t, u) = 0$, the equation (1) is called porous medium equation(PME) [36]. As is said in [36], if the initial condition has compact support, then (1) and (2) have at most one weak solution that has compact support in space (for more detail, see Theorem 5.3 of [36]). The degenerate parabolic equations appear often in applications, for example, spread of viscous fluids [11], mathematical biology [7], groundwater [6], heat transfer [16], flow of an isentropic gas through a porous medium [36], and other fields.

Methods for approximating solutions to (1) have attracted a lot of attention in recent years, for example, local discontinuous Galerkin finite element method [39], relaxation scheme [9], and kinetic scheme [4] have been proposed to find its solution. Also, Liu, Shu, and Zhang [26] proposed two different formulations of WENO schemes for solving nonlinear degenerate parabolic equations. The first formulation approximates directly the second derivative term by using a conservative flux difference, while the second formulation is similar to the formulation of the local discontinuous Galerkin (LDG) schemes [10].

As we know, WENO schemes were introduced in the literature to approximate hyperbolic conservation laws. Also, WENO schemes are based upon the essentially nonoscillatory (ENO) schemes [17]. The first version of WENO schemes was introduced in finite volume formulation for the one-dimensional conservation laws in 1994 by Liu, Osher, and Chan [25]. In 1996, Jiang and Shu observed that the ENO stencil selection is sensitive to the round-off perturbation near zeros of the solution and its derivatives [21]. Then, they improved the ENO reconstruction and proposed a general framework for designing arbitrary order accurate finite difference WENO schemes, which are more efficient for multidimensional calculations.

The degenerate parabolic equation (1) may have discontinuous solution, possible existence of sharp fronts, and finite speed of propagation of wave fronts [36]. The degenerate parabolic equations usually have features similar to those of a hyperbolic conservation laws. Therefore for solving (1), it is reasonable to generalize numerical methods for solving hyperbolic conservation laws, such as the WENO schemes [26].

In this paper, a WENO finite difference scheme is proposed by following the idea of the local discontinuous Galerkin method [10]. First rewrite (1) in one-dimensional case as a nonlinear system of first order equations

$$\begin{aligned} u_t &= v_x + S(x, t, u) \\ v &= b(u)_x, \end{aligned}$$

and then to solve the two first order equations using a fifth order finite difference WENO method for conservation laws. This approach has the advantage of simplicity, and it is easier to generalize it to higher than second order PDEs.

The structure of this paper is as follows: In section 2, we describe by detailing the construction and implementation of the scheme, for nonlinear degenerate parabolic equations. In section 3, the results of numerical experiments conducted with the proposed scheme are given. Some remarks are made in section 4.

2 Nonoscillatory reconstruction to the second derivative

In this section, a fifth-order WENO finite difference scheme for multidimensional nonlinear degenerate parabolic equation is described. Using the dimension by dimension approach [32], the presented scheme in this paper for multidimensional problems is implemented.

2.1 General framework

Consider the one-dimensional nonlinear degenerate parabolic equation

$$\begin{aligned} &u_t = b(u)_{xx} + S(x,t,u), \qquad (x,t) \in \Omega \times (0,\infty), \\ &u(x,0) = u_0(x), \end{aligned} \tag{3}$$

satisfying suitable boundary conditions.

This section describe the formulation of a WENO finite difference scheme by following the idea of the local discontinuous Galerkin method [10]. First, the equation (3) is considered as a nonlinear system of first order equations

$$u_t = v_x + S(x,t,u) \tag{4}$$

$$v = b(u)_x, \tag{5}$$

and then to solve the two first order equations, respectively, using the fifth order finite difference WENO method for conservation laws [1]. This approach has the advantage of simplicity, and it is easy to generalize it to higher than second order PDEs. The effective stencil, which is a composition of two successive WENO procedures, is also wider in comparison with the approach that is said in [2]. To make the final effective stencil smaller, a right-biased stencil for (4) followed by a left-biased stencil for (5) is used.

2.2 The fifth order finite difference WENO method

Assuming that the cell averages $\bar{u}_j$ are known at time t, van Leer [35] proposed a piecewise polynomial reconstruction $u(x,t) = \sum_j R_j(x)\chi_j(x)$ to solve 1-dimension hyperbolic conservation laws, where $\chi_j(x)$ is the characteristic function of the cell $I_j = [x_{j-\frac{1}{2}}, x_{j+\frac{1}{2}}]$. Let $U(x)$ be the primitive function of $u(x,t)$; that is, $U(x) = \int_{-\infty}^{x} u(\xi,t)d\xi$. To begin, an optimal polynomial is selected, which is denoted by $p_{\text{opt},j}(x)$, to approximate $u(x,t)$ on cell I_j of degree four on the five-cells central stencil $S \equiv \{I_{j-2}, \ldots, I_{j+2}\}$. In [30, 32], this optimum polynomial is obtained. First, $U(x)$ is interpolated at the cell boundaries $\{x_{j-\frac{5}{2}}, \ldots, x_{j+\frac{5}{2}}\}$ by using Newton's interpolation formula. Afterwards, differentiating the new polynomial, we get

$$p_{\text{opt},j}(x) = \sum_{i=1}^{5} U[x_{j-\frac{5}{2}}, \ldots, x_{j+i-\frac{5}{2}}] \sum_{m=0}^{i-1} \prod_{l=0, l\neq m}^{i-1} (x - x_{j+l-\frac{5}{2}}),$$

where $U[\cdots]$ is a divided difference of the function $U(x)$. High-order ENO reconstructions decrease damping of the solution, but generate significant oscillations when solving hyperbolic systems unless costly characteristic decompositions are used. For solving this problem, three supplementary polynomials are defined, $\{p_0^j(x), p_1^j(x), \text{and } p_2^j(x)\}$, approximating $u(x)$ with a lower accuracy on I_j. The three-cells stencils of ENO3 are obtained by either choosing r cells to the left and s cells to the right of I_j. Then, the three-cells stencils of ENO3 can be explicitly determined.

$$S^r \equiv \{I_{j-r}, \ldots, I_{j+s}\}, \qquad (r,s) = (0,2), (1,1), \text{ and } (2,0).$$

Having obtained $p_{opt}(x)$ as above, $p^{(r),j}(x)$ is obtained from cell boundaries of the stencil S^r

$$p^{(r),j}(x) = \sum_{i=1}^{3} U[x_{j-r-\frac{1}{2}}, \ldots, x_{j-r+i-\frac{1}{2}}] \sum_{m=0}^{i-1} \prod_{l=0, l\neq m}^{i-1} (x - x_{j-r+l-\frac{1}{2}}). \quad (6)$$

In order to obtain a more efficient reconstruction, the ENO3 reconstruction is modified. We interpolate equation (6) over an additional point lying within the same stencil and the same number of selection steps as ENO3. The new reconstruction starts by seeking a new high-order interpolating polynomial, $p_r^j(x)$, such that equation (6) passes over the additional point $x_j \in I_j$,

$$p_r^j(x) = p^{(r),j}(x) + U[x_{j-r-\frac{1}{2}}, \ldots, x_{j-r+\frac{5}{2}}, x_j] \sum_{m=0}^{3} \prod_{l=0, l\neq m}^{3} (x - x_{j-r+l-\frac{1}{2}}), \; r = 0,1,2. \quad (7)$$

The divided difference $U[x_{j-r+\frac{5}{2}}, x_j]$, for $r = 0, 1$, and 2 of (7), is given by

$$\begin{aligned} U[x_{j-r+\frac{5}{2}}, x_j] &= \tfrac{1}{x_j - x_{j-r+\frac{5}{2}}} \left[\int_{-\infty}^{x_j} u(\xi) d\xi - \int_{-\infty}^{x_{j-r+\frac{5}{2}}} u(\xi) d\xi \right] \\ &= \tfrac{1}{x_j - x_{j-r+\frac{5}{2}}} \int_{x_{j-r+\frac{5}{2}}}^{x_j} \left(\textstyle\sum_j L_j(x) \chi_j(x) \right) dx. \end{aligned} \tag{8}$$

As it can be seen from the equation (8), a polynomial that retains information within the cell I_j is needed. The NT scheme [29] is based on the first-order Lax–Friedrichs scheme [13] and it involves the reconstruction of piecewise-linear MUSCL-type interpolates from piecewise constant data and uses nonlinear limiters to prevent oscillations

$$L_j(x) = \bar{u}_j + (x - x_j) \frac{1}{h} u'_j, \quad x \in I_j. \tag{9}$$

Integrating over (9), the divided differences in (8) are given by

$$U[x_{j-r+\frac{5}{2}}, x_j] = \frac{1}{5-2r} \Bigg(\bar{u}_j - (r^2 - r - 2)\bar{u}_{j+1} + (r^2 - 3r + 2)\bar{u}_{j+2} + \frac{1}{4} u'_j \Bigg), \quad r = 0, 1, 2.$$

For the numerical derivative u'_j, the UNO limiter [18] is chosen which is given by

$$u'_j = \mathbf{MM} \Bigg(\Delta \bar{u}_{j-\frac{1}{2}} + \frac{1}{2} \mathbf{MM}(\Delta^2 \bar{u}_{j-1}, \Delta^2 \bar{u}_j), \Delta \bar{u}_{j+\frac{1}{2}} - \frac{1}{2} \mathbf{MM}(\Delta^2 \bar{u}_j, \Delta^2 \bar{u}_{j+1}) \Bigg),$$

where $\Delta^2 \bar{u}_j = \Delta \bar{u}_{j+\frac{1}{2}} - \Delta \bar{u}_{j-\frac{1}{2}}$, and $\Delta \bar{u}_{j+\frac{1}{2}} = \bar{u}_{j+1} - \bar{u}_j$. Here, the MinMod limiter (**MM**) is defined by

$$\mathbf{MM}(x_1, x_2, \ldots) = \begin{cases} \min_p \{x_p\} & \text{if } x_p > 0, \\ \max_p \{x_p\} & \text{if } x_p < 0, \\ 0 & \text{otherwise.} \end{cases}$$

2.3 Essentially nonoscillatory reconstruction

Spurious oscillations can appear in the numerical solution, if the big stencil which defines $p_{\text{opt},j}(x)$, contains a discontinuity or large gradients. To avoid

such a problem a WENO procedure is designed that smoothly adapts the stencil in the neighbourhood of the singularity.

The principle of CWENO (central WENO) procedure which is defined in [8, 24] is extended, and an ENO interpolant is constructed as a convex combination of polynomials that are based on different stencils; that is,

$$R_j(x) \equiv \sum_i w_i^j p_i^j(x), \qquad w_i^j \geq 0, \ \sum_i w_i^j = 1, \ i \in \{0,1,2,c\}. \tag{10}$$

Here, $R_j(x)$ is the nonoscillatory reconstruction on I_j. $p_c^j(x)$ is a polynomial which is defined on stencil S, also the polynomials $p_0^j(x), p_1^j(x)$, and $p_2^j(x)$ are computed in (7). In order to simplify the notations, the upper index j will be omitted; remembering that the weights and the four polynomials change from cell to cell. Now, the polynomial $p_c(x)$ is computed such that the convex combination (10), will be fifth-order accurate in smooth regions. It must, therefore, satisfy the following equation:

$$p_{\text{opt}}(x) = C_0 p_0(x) + C_1 p_1(x) + C_2 p_2(x) + C_c p_c(x), \quad \sum_i C_i = 1 \ i \in \{0,1,2,c\}, \tag{11}$$

where constants C_i represent linear or ideal weights for (10). A straightforward calculation shows that any symmetric choice of constants C_i in (11) provides the desired accuracy. This property must be contrasted with classical upwind WENO schemes. Therefore, we make the choice $C_0 = C_2 = \frac{1}{8}, C_1 = \frac{1}{4}$, and $C_c = \frac{1}{2}$. Then, the polynomial $p_c(x)$ is obtained explicitly as follows:

$$p_c(x) = [p_{\text{opt}}(x) - C_0 p_0(x) - C_1 p_1(x) - C_2 p_2(x)]/C_c \qquad \forall x \in I_j. \tag{12}$$

In order to complete the reconstruction of $R_j(x)$, the ideal weights C_i, $i \in \{0,1,2,c\}$, are changed to nonlinear weights w_i, with objective of maintaining the fifth-order accuracy for smooth solutions and nonoscillatory performance near discontinuities. In smooth regions for achieving the optimal interpolation (11), the weights w_i must smoothly converge to the ideal weights C_i as h approaches zero. Also, in regions where a discontinuity does exist, the weights should effectively remove the contribution of stencils that contain the discontinuity.

2.4 The nonoscillatory weights

In order to fully determine the scheme, it is required to specify the nonoscillatory weights,. Then, following [21,32], the nonlinear weights are written as

$$w_i = \frac{\alpha_i}{\sum_k \alpha_k}, \quad \alpha_i = \frac{C_i}{(\epsilon + IS_i)^2}, \quad i,k \in \{0,1,2,c\}. \tag{13}$$

The constants $C_i,\ i \in \{0,1,2,c\}$, in Eq. (13) are chosen to be the same as in the equation (11); that is, $C_0 = C_2 = \frac{1}{8}, C_1 = \frac{1}{4}$, and $C_c = \frac{1}{2}$.

The *smoothness indicators*, IS_i, are responsible for detecting large gradients or discontinuities and automatically switch to the stencil that generates the least oscillatory reconstruction in such cases. The smoothness indicator is defined as [21]

$$IS_i = \sum_k h^{2k-1} \times \int_{I_j} \left(\frac{d^k}{dx^k} p_i(x)\right)^2 dx, \qquad i \in \{0,1,2,c\}.$$

The constant ϵ, taken to prevent the denominator from vanishing, can range from 10^{-5} to 10^{-7}, [21]. As is said in [12] and [19], different values of ϵ change the order of convergence of the scheme and yield different sharpness near discontinuities. In this paper, $\epsilon = 10^{-6}$ is used. The smoothness indicators of smooth and discontinuous stencils yield $IS_r = \mathcal{O}(h^2)$ and $IS_r = \mathcal{O}(1)$, respectively. A direct computation based on equations (7) and (12) yields:

$$\begin{aligned} IS_r =& \frac{1}{8100}(9\bar{u}_j - 12\bar{u}_{j+(1-r)} + 3\bar{u}_{j+2(1-r)} + (1-r)96u'_j)^2 \\ &+ \frac{13}{2700}(57\bar{u}_j - 66\bar{u}_{j+(1-r)} + 9\bar{u}_{j+2(1-r)} + (1-r)48u'_j)^2 \\ &+ \frac{781}{162000}(72\bar{u}_j - 96\bar{u}_{j+(1-r)} + 24\bar{u}_{j+2(1-r)} + (1-r)48u'_j)^2, \quad r = 0,2, \end{aligned}$$

$$\begin{aligned} IS_1 =& \frac{9}{2916}(\bar{u}_{j-1} - \bar{u}_{j+1} - 16u'_j)^2 + \frac{13}{12}(\bar{u}_{j-1} - 2\bar{u}_j + \bar{u}_{j+1})^2 \\ &+ \frac{449856}{58320}(\bar{u}_{j-1} - \bar{u}_{j+1} + 2u'_j)^2, \end{aligned}$$

and

$$\begin{aligned} IS_c =& (\frac{23957}{31500}\bar{u}_{j+2} - \frac{690709}{126000}\bar{u}_{j+1} + \frac{34913}{8400}\bar{u}_j - \frac{4051}{126000}\bar{u}_{j-1} - \frac{20591}{126000}\bar{u}_{j-2})\bar{u}_{j+2} \\ &+ (\frac{1478263}{126000}\bar{u}_{j+1} - \frac{7423}{350}\bar{u}_j + \frac{68419}{21000}\bar{u}_{j-1} - \frac{4051}{126000}\bar{u}_{j-2})\bar{u}_{j+1} \\ &+ (\frac{143239}{8400}\bar{u}_j - \frac{7423}{350}\bar{u}_{j-1} + \frac{34913}{8400}\bar{u}_{j-2})\bar{u}_j \\ &+ (\frac{1478263}{126000}\bar{u}_{j-1} - \frac{690709}{126000}\bar{u}_{j-2})\bar{u}_{j-1} + (\frac{23957}{31500}\bar{u}_{j-2})\bar{u}_{j-2} \\ &+ (\frac{2464}{1125}u'_j - \frac{649}{375}\bar{u}_{j-2} + \frac{2486}{375}\bar{u}_{j-1} - \frac{2486}{375}\bar{u}_{j+1} + \frac{649}{375}\bar{u}_{j+2})u'_j. \end{aligned}$$

2.5 The new scheme for nonlinear degenerate parabolic PDEs

From equations (4) and (5), it is required to approximate $b(u)_x$ and v_x. The final form of the left- and right-biased points are given by

$$u^-_{j+\frac{1}{2}} = \sum_{i\in\{0,1,2,c\}} w_i \times u^{-(i)}(x_{j+\frac{1}{2}}),$$

$$v^+_{j-\frac{1}{2}} = \sum_{i\in\{0,1,2,c\}} w_i \times v^{+(i)}(x_{j-\frac{1}{2}}),$$

where

$$u^{-(0)}_{j+\frac{1}{2}} := p_0(x_{j+\frac{1}{2}}) = (22\bar{u}_j + 9\bar{u}_{j+1} - \bar{u}_{j+2} + 8u'_j)/30,$$

$$u^{-(1)}_{j+\frac{1}{2}} := p_1(x_{j+\frac{1}{2}}) = (\bar{u}_{j-1} + 15\bar{u}_j + 2\bar{u}_{j+1} + 8u'_j)/18,$$

$$u^{-(2)}_{j+\frac{1}{2}} := p_2(x_{j+\frac{1}{2}}) = (-2\bar{u}_{j-2} + 13\bar{u}_{j-1} + 19\bar{u}_j + 24u'_j)/30,$$

$$\begin{aligned} u^{-(c)}_{j+\frac{1}{2}} &:= p_c(x_{j+\frac{1}{2}}) \\ &= (30\bar{u}_{j-2} - 205\bar{u}_{j-1} + 291\bar{u}_j + 277\bar{u}_{j+1} - 33\bar{u}_{j+2} - 176u'_j)/360, \end{aligned}$$

and

$$v^{+(0)}_{j-\frac{1}{2}} := p_0(x_{j-\frac{1}{2}}) = (19\bar{v}_j + 13\bar{v}_{j+1} - 2\bar{v}_{j+2} - 24v'_j)/30,$$

$$v^{+(1)}_{j-\frac{1}{2}} := p_1(x_{j-\frac{1}{2}}) = (2\bar{v}_{j-1} + 15\bar{v}_j + \bar{v}_{j+1} - 8v'_j)/18,$$

$$v^{+(2)}_{j-\frac{1}{2}} := p_2(x_{j-\frac{1}{2}}) = (-\bar{v}_{j-2} + 9\bar{v}_{j-1} + 22\bar{v}_j - 8v'_j)/30,$$

$$\begin{aligned} v^{+(c)}_{j-\frac{1}{2}} &:= p_c(x_{j-\frac{1}{2}}) \\ &= (-33\bar{v}_{j-2} + 277\bar{v}_{j-1} + 291\bar{v}_j - 205\bar{v}_{j+1} + 30\bar{v}_{j+2} + 176v'_j)/360. \end{aligned}$$

Therefore,

$$\begin{cases} \bar{v}_j = \frac{b(u^-_{j+\frac{1}{2}}) - b(u^-_{j-\frac{1}{2}})}{h}, \\ \frac{d\bar{u}_j(t)}{dt} = \frac{v^+_{j+\frac{1}{2}} - v^+_{j-\frac{1}{2}}}{h} + S(x_j, t, u_j) = F(\bar{u}_j(t)), \end{cases} \tag{14}$$

and the semidiscrete scheme (14) is discretized in time by a third order TVD RungeKutta method [33], which is given by

$$\begin{aligned}
\bar{u}_j^{(1)} &= \bar{u}_j^n + \Delta t F(\bar{u}_j^n), \\
\bar{u}_j^{(2)} &= \tfrac{3}{4}\bar{u}_j^n + \tfrac{1}{4}\bar{u}_j^{(1)} + \tfrac{1}{4}\Delta t F(\bar{u}_j^{(1)}), \\
\bar{u}_j^{n+1} &= \tfrac{1}{3}\bar{u}_j^n + \tfrac{2}{3}\bar{u}_j^{(2)} + \tfrac{2}{3}\Delta t F(\bar{u}_j^{(2)}).
\end{aligned} \tag{15}$$

3 Numerical results

This section gives some numerical examples to confirm the accuracy, robustness, and high-resolution properties of the proposed method. Example 1 is three-dimensional heat equation with a known exact solution and is used for checking the accuracy and order of convergence [15]. Example 2 is the two-dimensional porous medium equation [26]. In Example 3, a nonlinear problem is presented and suggested as test for multidimensional nonlinear convection-diffusion problems [3, 22]. Next, in Example 4, a scalar two-dimensinal reaction-diffusion equation is considered [7]. Example 5 taken from [20, 23], is presented to cover the case strongly degenerate parabolic equation. Finally, Example 6 is considered to solve a Turing model of biological pattern formation [7]. This example will demonstrate that the new technique also handles systems of degenerate equations. The constant CFL number $c = 0.3$ is considered. Then, the time step is determined by

$$\max_u |b'(u)| \frac{\Delta t}{h^2} = 0.3.$$

Also, in the following, CWENO5 is used to denote the new proposed method in the current paper.

Example 1. For $\mathbf{x} = (x, y, z)$, $S(\mathbf{x}, t, u) \equiv 0$, and $b_j(u) = u$, $j = 1, 2, 3$, consider the three-dimensional linear initial-value problem with periodic boundary condition [15],

$$\begin{cases} u_t = u_{xx} + u_{yy} + u_{zz}, \ \mathbf{x} \in \Omega = (-\pi, \pi)^3, \ t > 0, \\ u(x, y, z, 0) = \sin(x)\sin(y)\sin(z). \end{cases}$$

The closed analytical form solution for this problem is

$$u(x, y, z, t) = \exp(-t)\sin(x)\sin(y)\sin(z).$$

The error is computed in the discrete L_∞ and L_1 norms and, respectively, defined by

$$||u||_\infty = \max_{i,j,k} |u_{i,j,k}|,$$

$$||u||_1 = \sum_{i,j,k} |u_{i,j,k}| \Delta x^3.$$

Table 1: Errors for Example 1 at T=2

N	L_∞ error	L_∞ order	L_1 error	L_1 order	CPU
10	0.192(-2)	-	0.847(-3)	-	08.97
20	0.601(-4)	5.000	0.266(-4)	4.999	15.01
40	0.189(-5)	4.999	0.822(-6)	5.021	32.84
80	0.579(-7)	5.030	0.257(-7)	5.000	68.10
160	0.163(-8)	5.151	0.804(-9)	5.000	142.90

Table 2: Errors and orders of convergence for Example 1 with different linear weights at T=2. Top:$C_0 = C_1 = C_2 = C_c = \frac{1}{4}$, Middle:$C_0 = C_2 = \frac{1}{16}, C_1 = \frac{1}{2}, C_c = \frac{3}{8}$, Bottom:$C_0 = \frac{1}{4}, C_1 = C_2 = \frac{1}{8}, C_c = \frac{1}{2}$.

N	L_∞ error	L_∞ order	L_1 error	L_1 order	CPU
10	0.115(-2)	-	0.788(-3)	-	09.12
20	0.400(-4)	4.845	0.295(-4)	4.739	15.15
40	0.110(-5)	5.184	0.910(-6)	5.018	33.01
80	0.347(-7)	4.986	0.290(-7)	4.971	70.11
160	0.107(-8)	5.019	0.863(-9)	5.070	139.98
10	0.149(-2)	-	0.102(-2)	-	10.01
20	0.453(-4)	5.039	0.341(-4)	4.902	14.93
40	0.190(-5)	4.575	0.971(-6)	5.134	30.99
80	0.338(-7)	5.812	0.281(-7)	5.110	73.12
160	0.103(-8)	5.036	0.877(-9)	5.001	138.88
10	0.171(-2)	-	0.145(-2)	-	11.55
20	0.148(-3)	3.530	0.139(-3)	3.382	16.01
40	0.170(-4)	3.122	0.182(-4)	2.933	32.18
80	0.125(-5)	3.765	0.201(-5)	3.178	69.87
160	0.873(-7)	3.839	0.156(-6)	3.687	140.11

In Table 1, the respective errors and convergence rates by CWENO5 are given. The results verify the fifth-order accuracy both in the L_∞ and in the L_1 norms. The L_1 and L_∞ errors and orders of convergence by CWENO5 with different linear weights are reported in Table 2. As is expected, any symmetric choice of constants C_i enables the fifth-order accuracy.

Example 2. Consider the porous medium equation (PME) as [26]

$$u_t = \Delta(u^m), \qquad m > 1, \tag{16}$$

where $u = u(\mathbf{x}, t)$, $\mathbf{x} \in \Omega \subset \mathbb{R}^d$. This equation describes various diffusion processes, such as the flow of an isentropic gas through a porous medium where u is the density of the gas required to be non-negative and u^{m-1} is the pressure of the gas. The PME equation degenerates at points where $u = 0$,

Table 3: Errors and orders of convergence for Example 2 at T=2. Top to Bottom respectively: $m = 2,\ m = 4,\ m = 6$, and $m = 8$.

N	L_∞ error	L_∞ order	L_1 error	L_1 order	CPU
50	0.012(-1)	-	0.429(-1)	-	10.62
100	0.010(-1)	0.263	0.172(-1)	1.318	19.88
200	0.006(-1)	0.737	0.036(-1)	2.256	35.17
400	0.002(-1)	1.585	0.006(-1)	2.585	78.41
50	0.117(-1)	-	0.248	-	13.51
100	0.083(-1)	0.495	0.639(-1)	1.956	23.23
200	0.069(-1)	0.266	0.256(-1)	1.319	37.11
400	0.054(-1)	0.353	0.092(-1)	1.476	86.12
50	0.216(-1)	-	0.353	-	16.55
100	0.232(-1)	-0.103	0.135	1.386	27.51
200	0.179(-1)	0.374	0.725(-1)	0.896	41.68
400	0.134(-1)	0.417	0.248(-1)	1.547	95.90
50	0.337(-1)	-	0.583	-	23.55
100	0.248(-1)	0.442	0.201	1.536	39.77
200	0.213(-1)	0.219	0.752(-1)	1.418	53.13
400	0.218(-1)	-0.033	0.368(-1)	1.031	115.55

resulting in the phenomenon of finite speed of propagation and sharp fronts. The classical solutions to the PME may not exist in general, even if the initial condition is smooth. The closed analytical form which is a weak solution for PME, is obtained by Zel'dovich and Kompaneets [38] and Barenblatt [5] in years 1950 and 1952, respectively. The solution of [5] has the following explicit form

$$u(\mathbf{x},t) = t^{-\alpha}\left[\left(1 - k|\mathbf{x}|^2 t^{-\frac{2\alpha}{d}}\right)_+\right]^{\frac{1}{m-1}}, \tag{17}$$

where $\alpha = \frac{d}{(m-1)d+2}$, $k = \frac{\alpha(m-1)}{2md}$, and $u_+ = \max(u, 0)$. Now, we put $d = 2$; therefore, Barenblatt solution has no derivative at the points of the circle $x^2 + y^2 = \sqrt{\frac{4m}{\alpha(m-1)}}t^\alpha$, where $\alpha = \frac{1}{m}$. The CWENO5 scheme is used to solve the PME (16) for $m = 2, 4, 6$ and $m = 8$, where $\Omega = [-10, 10]^2$. The initial condition is taken as the Barenblatt solution (17) at $t = 1$, and the boundary condition is chosen to be $u = 0$ on $\partial\Omega$ for $t > 1$.

Table 3 indicates the magnitude of errors obtained with CWENO5 scheme for different mesh sizes. Figure 1 shows the results of CWENO5 scheme at the Final time $T = 3$ with the computational domain Ω divided into 120 uniform cells. The CWENO5 scheme prevents the appearance of spurious solutions close to the circles. The contour plots of absolute difference between approximated solution and Barenblatt solution with $m = 2, 4$ are shown in Figure 1 top right and bottom right, respectively. The CWENO5 scheme is sufficiently

Table 4: Errors and orders of convergence for Example 2 ($m = 2$) with different linear weights at T=2. Top:$C_0 = C_1 = C_2 = C_c = \frac{1}{4}$, Middle:$C_0 = C_2 = \frac{1}{16}, C_1 = \frac{1}{2}, C_c = \frac{3}{8}$, Bottom:$C_0 = \frac{1}{4}, C_1 = C_2 = \frac{1}{8}, C_c = \frac{1}{2}$.

N	L_∞ error	L_∞ order	L_1 error	L_1 order	CPU
50	0.012(-1)	-	0.422(-1)	-	10.89
100	0.009(-1)	0.415	0.165(-1)	1.354	20.85
200	0.005(-1)	0.848	0.037(-1)	2.156	34.37
400	0.002(-1)	1.322	0.007(-1)	2.402	80.51
50	0.014(-1)	-	0.418(-1)	-	11.11
100	0.008(-1)	0.807	0.167(-1)	1.324	22.20
200	0.006(-1)	0.415	0.039(-1)	2.098	33.01
400	0.003(-1)	1.000	0.009(-1)	2.116	81.52
50	0.222(-1)	-	0.338	-	09.95
100	0.218(-1)	0.026	0.165	1.035	22.51
200	0.157(-1)	0.473	0.722(-1)	1.192	35.68
400	0.131(-1)	0.261	0.243(-1)	1.571	79.95

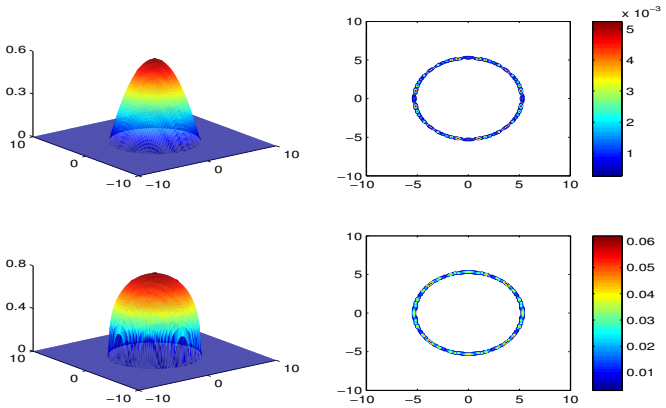

Figure 1: Example 2 (two-dimensional porous medium equation). Top left: PME with $m = 2$ and $N = 120$, Top right: 30 contour lines of $|u_{\text{Barenblatt}} - u|$ with $m = 2$, Bottom left: PME with $m = 4$ and $N = 120$, Bottom right: 30 contour lines of $|u_{\text{Barenblatt}} - u|$ with $m = 4$.

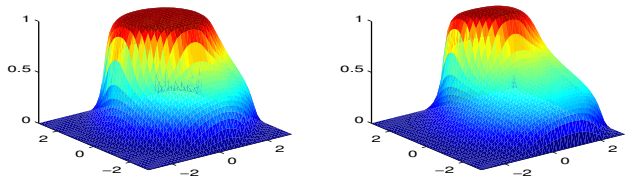

Figure 2: Example 3 (two-dimensional Buckley–Leverett-type equation). Left: numerical solution at $T = 0.5$ with $N = 40$, Right: numerical solution at $T = 1.0$ with $N = 40$.

accurate in the smooth regions, while on the nonsmooth regions absolute difference with analytical form solution of Barenblatt is of order 10^{-3} and 10^{-2} for $m = 2$ and $m = 4$, respectively.

Example 3. This example solves the Buckley–Leverett-type problem [3, 22]

$$u_t + f(u)_x + g(u)_y = \epsilon(u_{xx} + u_{yy})$$

with $\epsilon = 0.1$, the flux function of the form

$$g(u) = \frac{u^2}{u^2 + (1-u)^2},$$

$$f(u) = g(u)(1 - 5(1-u)^2).$$

The initial function for this example is

$$u(x, y, 0) = \begin{cases} 1, & (x-0.25)^2 + (y-0.25)^2 < 5, \\ 0, & otherwise. \end{cases}$$

This example includes gravitational effects in the x-direction. The numerical results at $T = 0.5$ and 1.0 are shown in Figure 2, with the computational domain $[-3, 3]^2$ divided into 40×40 uniform cells. The results compare well with those reported in [3]. Table 5 gives the respective errors and convergence rates by CWENO5. The numerical solutions compared with a "reference solution", obtained by WENO6 [26] with $N = 400$.

Example 4. This example solves the following initial-boundary-value problem for a scalar reaction-diffusion equation [7], where $\mathbf{x} = (x, y)$,

$$u_t = \Delta b(u) + S(\mathbf{x}, t, u), \tag{18}$$

$$u(\mathbf{x}, 0) = 0.5(1 + \sin(1.1(x - \cos(0.7y)))) \cos(0.5(y - \sin(1.3x))),$$

$$\nabla b(u) \cdot \mathbf{n} = 0 \quad \text{on } \partial\Omega \times [0, T]. \tag{19}$$

Table 5: Errors and orders of convergence for Example 3 at T=0.5

N	L_∞ error	L_∞ order	L_1 error	L_1 order	CPU
40	0.228(-3)	-	0.716(-4)	-	33.63
80	0.680(-5)	4.987	0.248(-5)	4.852	58.12
160	0.215(-6)	4.998	0.799(-7)	4.955	109.87
320	0.671(-8)	4.992	0.239(-8)	5.060	219.23

This problem may serve as a scalar prototype degenerate reaction-diffusion model. Here, the zero-flux boundary condition (19) implies that the reaction-diffusion domain is isolated from the external environment. For $S(\mathbf{x}, t, u) = S(u)$, (18) appears in [28] in an ecological setting, where u denotes the population density of a species, and $S(u)$ is its dynamics, where it is assumed that $S(0) = 0$ and $S'(0) \neq 0$. For example, $S(u) = u(1-u) - u^2/(1+u^2)$ corresponds to the population dynamics of the spruce band-worm [28] and models the growth of the population by a logistic expression and the rate of mortality due to predation by other animals. Authors of [7] modified this expression by a radial spatial factor, and used

$$S(\mathbf{x}, t, u) = 10(\exp(-5r)u(1-u) + (\exp(-5r) - 1)\frac{u^2}{1+u^2}),$$
$$r = \sqrt{(x-0.5)^2 + (y-0.5)^2},$$

which means that the birth of individuals is concentrated near the centre $(0.5, 0.5)$, and mortality increases with increasing distance from the centre. Most standard spatial models of population dynamics simply assume that $b(u) = Du$, where the constant diffusion coefficient $D > 0$ measures the dispersal efficiency of the species under consideration. In this example, the strongly degenerate diffusion coefficient [7, 37] is used

$$b(u) = \begin{cases} 0, & u \leq u_c, \\ D(u - u_c), & otherwise, \end{cases}$$

where $u_c > 0$ is an assumed critical value of u beyond which diffusion will take place. Here, we set $D = 1$ and $u_c = \frac{1}{2}$. The difficulty in the well-posedness analysis of the problem (18) lies in the boundary condition (19) when b is strongly degenerate. It is quite difficult to give a correct formulation of the zero-flux boundary conditions. The computational domain $[0, 1]^2$ is divided into 80×80 uniform cells. Figure 3 shows the numerical approximation at different time levels. The results compare well with those reported in [7].

Example 5. In this example, we focus on strongly degenerate parabolic problem. Consider the Burgers-like equation

$$u_t + (u^2)_x + (u^2)_y = \epsilon(\nu(u)u_x)_x + \epsilon(\nu(u)u_y)_y.$$

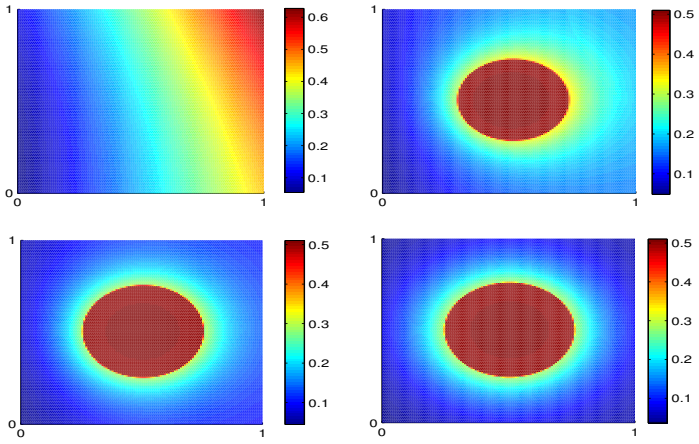

Figure 3: Example 4 (single-species reaction-diffusion model). From top left to bottom right, it shows the numerical solution at times $T = 0.0,\ 0.5,\ 1.0,\ 3.0$.

Table 6: Errors and orders of convergence for example 5 at T=0.5

N	L_∞ error	L_∞ order	L_1 error	L_1 order	CPU
40	0.223(-4)	-	0.118(-4)	-	30.73
80	0.715(-6)	4.963	0.362(-6)	5.000	53.98
160	0.214(-7)	5.059	0.112(-7)	5.014	100.11
320	0.599(-9)	5.162	0.334(-9)	5.054	213.23

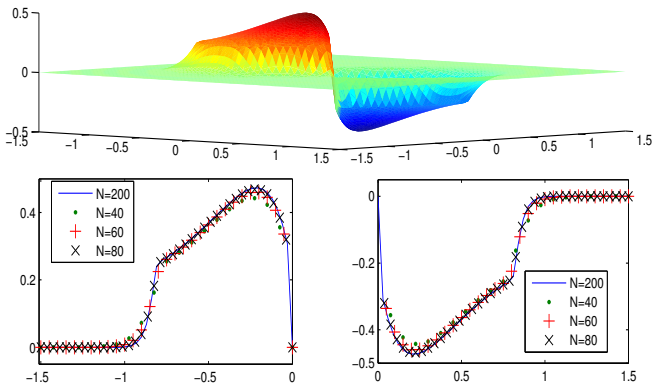

Figure 4: Example 5 (two-dimensional strongly degenerate parabolic problem). Top: numerical solution at $T = 0.5$ with $N = 80$, Bottom: one-dimensional cut along the y axis with different mesh sizes.

Here, $\epsilon = 0.1$ is considered and

$$\nu(u) = \begin{cases} 0, & |u| \leq 0.25, \\ 1, & |u| > 0.25. \end{cases}$$

In this example, zero boundary conditions are applied. The initial condition is equal to -1 and 1 inside two circles of radius 0.4 centred at $(0.5, 0.5)$ and $(-0.5, -0.5)$, respectively, and is zero elsewhere inside the square $[-1.5, 1.5]^2$. The L_∞ and L_1 errors of CWENO5 scheme are given in Table 6 for different mesh sizes. The computational domain is divided into 80×80 uniform cells. The numerical results obtained by CWENO5 scheme are presented in Figure 4, which compare well with those reported in [23,26]. The "reference solution" was obtained by WENO6 [26] scheme with $N = 400$.

Example 6. Turing [34] wrote his paper "The chemical basis of morphogenesis" in which he suggested an new theory. He hypothesized that the patterns, observed during embryonic development, occur in reaction to a spatial prepattern in biochemicals, which he termed morphogens. Cells would then answer to this prepattern by differentiating in a threshold-dependent way. Thus, Turing hypothesized that the patterns, observed in nature, such as pigmentation in animals, branching in trees, and skeletal structures are reflections of inhomogeneities in underlying biochemical signalling.

The system he considered took the form

$$\frac{\partial \mathbf{u}}{\partial t} = \mathbf{D}\nabla^2 \mathbf{u} + \mathbf{f}(\mathbf{u}).$$

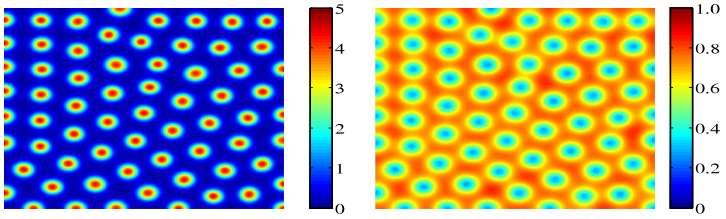

Figure 5: Example 6 (Turing's model for biological pattern formation). Left: u after 1113 simulated time units, Right: v after 1113 simulated time units.

Here, $\mathbf{u}$ is a vector of chemical condensations, $\mathbf{D} = \begin{bmatrix} D_u & 0 \\ 0 & D_v \end{bmatrix}$ is a matrix constant diffusion coefficients, and the nonlinear function $\mathbf{f}(\mathbf{u})$ is the reaction kinetics. Turing analysed the special case of equation (3) when there are two interacting morphogens, $\mathbf{u} = (u, v)^T$. They spread at rates D_u and D_v, respectively, and they also undergo reaction kinetics defined by $\mathbf{f}(\mathbf{u}) = (f(u, v), g(u, v))^T$. There are different forms of the reaction kinetics such as Gierer–Meinhardt [14] model

$$f(u, v) = c_1 - c_2 u + c_3 \frac{u^2}{(1 + ku^2)v}, \qquad g(u, v) = c_4 u^2 - c_5 v$$

and the Schnakenberg [31] model

$$f(u, v) = c_1 - c_{-1} u + c_3 u^2 v, \qquad g(u, v) = c_2 - c_3 u^2 v.$$

The parameters $\{c_{-1}, c_1, c_2, c_3\}$ represent the deterministic rates of the reactions. Now, consider the Schnakenberg model on the unit square domain $\Omega = [0, 1] \times [0, 1]$ with zero-flux boundary conditions. Let the parameter values be determined by $D_u = 1$, $D_v = 40$, $c_1 = 0.1$, $c_2 = 0.9, c_{-1} = 1$, and $c_3 = 1$. The initial conditions are random perturbations about the homogeneous steady state. This system has a uniform positive steady state (u^0, v^0), where $u^0 = c_1 + c_2$ and $v^0 = c_2/(c_1 + c_2)^2$. Figure 5 shows the formation of spot patterns. In this figure, the concentration values of u and v are illustrated which compare well with those reported in [27].

4 Conclusion

When applying the standard WENO idea, as Liu, Shu, and Zhang did in [26], in some cases (odd numbers of nodes in small stencils) the linear weights don't exist, and when they do exist, at least one of them is negative. In

this research, another strategy was used to circumvent these problems. This strategy consists in applying the idea of the local discontinuous Galerkin method. First, the degenerate parabolic equation was considered as a nonlinear system of first order equations, and then this system was solved using a fifth-order finite difference weighted essentially nonoscillatory (WENO) method for conservation laws. The Symmetrical WENO procedure of [1] for solving this system was used. It was observed that this procedure generates a fifth-order method in smooth regions and remains essentially nonoscillatory near discontinuities. Numerical examples showed that the new scheme can obtain fifth-order accuracy in smooth regions and prevent the appearance of spurious solutions close to discontinuities.

Acknowledgement

The author is very thankful to reviewers for carefully reading the paper, their comments and suggestions have improved the quality of the paper.

References

1. Abedian, R., Adibi, H., and Dehghan, M. *A high-order symmetrical weighted hybrid ENO-flux limiter scheme for hyperbolic conservation laws*, Comput. Phys. Commun. 185 (2014), no. 1, 106–127.

2. Abedian, R., Adibi, H., and Dehghan, M. *A high-order weighted essentially non-oscillatory (WENO) finite difference scheme for nonlinear degenerate parabolic equations*, Comput. Phys. Commun. 184 (2013), no. 8, 1874–1888.

3. Acosta, C. D. and Bürger, R. *Difference schemes stabilized by discrete mollification for degenerate parabolic equations in two space dimensions*, IMA J. Numer. Anal. 32 (2012), no, 4, 1509–1540.

4. Aregba-Driollet, D., Natalini, R., and Tang, S. *Explicit diffusive kinetic schemes for nonlinear degenerate parabolic systems*, Math. Comp. 73 (2004), no. 245. 63–94.

5. Barenblatt, G. I. *On some unsteady motions of a liquid or a gas in a porous medium*, (Russian) Akad. Nauk SSSR. Prikl. Mat. Meh. 16, (1952). 67–78.

6. Barenblatt, G. I., Bertsch, M., Chertock, A. E., and Prostokishin, V. M. *Self-similar intermediate asymptotics for a degenerate parabolic filtration-absorption equation*, Proc. Natl. Acad. Sci. U.S.A. 97 (2000), no. 18, 9844–9848.

7. Bendahmane, M., Bürger, R., Ruiz-Baier, R., and Schneider, K. *Adaptive multiresolution schemes with local time stepping for two-dimensional degenerate reaction-diffusion systems*, Appl. Numer. Math. 59 (2009), no. 7, 1668–1692.

8. Capdeville, G. *A central WENO scheme for solving hyperbolic conservation laws on non-uniform meshes*, J. Comput. Phys, 227 (2008), no. 5, 2977–3014.

9. Cavalli, F., Naldi, G., Puppo, G., and Semplice, M. *High order relaxation schemes for nonlinear degenerate diffusion problems*, SIAM J. Numer. Anal. 45 (2007), no. 5, 2098–2119.

10. Cockburn, B. and Shu, C. -W. *The local discontinuous Galerkin method for time-dependent convection-diffusion systems*, SIAM J. Numer. Anal. 35 (1998), no. 6, 2440–2463.

11. Davidovitch, B., Moro, E., and Stone, A. H. *Spreading of viscous fluid drops on a solid substrate assisted by thermal fluctuations*, Phys. Rev. Lett. 95 (2005), no. 24, 244–505.

12. Fedkiw, R., Merriman, B., and Osher, S. *Simplified discretization of systems of hyperbolic conservation laws containing advection equations*, J. Comput. Phys. 157 (2000), no. 1, 302–326.

13. Friedrichs, K. O. and Lax, P. D. *Systems of conservation equations with a convex extension*, Proc. Natl. Acad. Sci. U.S.A. 68 (1971), 1686–1688.

14. Gierer, A. and Meinhardt, H. *A theory of biological pattern formation*, Biol. Cybern. 12 (1972), no. 1, 30–39.

15. Hajipour, M. and Malek, A. *High accurate NRK and MWENO scheme for nonlinear degenerate parabolic PDEs*, Appl. Math. Model. 36 (2012), no. 9, 4439–4451.

16. Harley, C. *Asymptotic and dynamical analyses of heat transfer through a rectangular longitudinal fin*, J. Appl. Math. 2013, Art. ID 987327, 1–8.

17. Harten, A., Engquist, B., Osher, S., and Chakravarthy, S. *Uniformly high-order essentially nonoscillatory schemes, III*, J. Comput. Phys. 71 (1987), no. 2, 231–303.

18. Harten, A. and Osher, S. *Uniformly high-order accurate nonoscillatory schemes I*, SIAM J. Numer. Anal. 24 (1987), no. 2, 279–309.

19. Henrick, A. K., Aslam, T. D., and Powers, J. M. *Mapped weighted essentially nonoscillatory schemes: Achieving optimal order near critical points*, J. Comput. Phys. 207 (2005), no. 2, 542–567.

20. Holden, H., Karlsen, K. H., and Lie, K. -A. *Operator splitting methods for degenerate convection-diffusion equations II: Numerical examples with emphasis on reservoir simulation and sedimentation*, Comput. Geosci. 4 (2000), 287–322.

21. Jiang, G. S. and Shu, C. -W. *Efficient implementation of weighted ENO schemes*, J. Comput. Phys. 126 (1996), no. 1, 202–228.

22. Karlsen, K. H. and Risebro, N. H. *An operator splitting method for nonlinear convection-diffusion equations*, Numer. Math. 77 (1997), no. 3, 365–382.

23. Kurganov, A. and Tadmor, E. *New high-resolution central schemes for nonlinear conservation laws and convection-diffusion equations*, J. Comput. Phys. 160 (2000), no. 1, 241–282.

24. Levy, D., Puppo, G., and Russo, G. *Compact central WENO schemes for multidimensional conservation laws*, SIAM J. Sci. Comput. 22 (2000), no. 2, 656–672.

25. Liu, X. -D., Osher, S., and Chan, T. *Weighted essentially non-oscillatory schemes*, J. Comput. Phys. 115 (1994), no. 1, 200–212.

26. Liu, Y., Shu, C. -W., and Zhang, M. *High order finite difference WENO schemes for nonlinear degenerate parabolic equations*, SIAM J. Sci. Comput. 33 (2011), no. 2, 939–965.

27. Maini, P. K., Woolley, T. E., Baker, R. E., Gaffney, E. A., and Lee, S. S. *Turing's model for biological pattern formation and the robustness problem*, Interface focus 2 (2012), no. 4, 487–496.

28. Murray, J. D. *Mathematical Biology II: Spatial Models and Biomedical Applications*, Springer-Verlag, New York, 2003.

29. Nessyahu, H. and Tadmor, E. *nonoscillatory central differencing for hyperbolic conservation laws*, J. Comput. Phys. 87 (1990), no. 2, 408–463.

30. Peer, A. A. I., Dauhoo, M. Z., Gopaul, A., and Bhuruth, M. *A weighted ENO-flux limiter scheme for hyperbolic conservation laws*, Int. J. Comput. Math. 87 (2010), no. 15, 3467–3488.

31. Schnakenberg, J. *Simple chemical reaction systems with limit cycle behaviour*, J. Theoret. Biol. 81 (1979), no. 3, 389–400.

32. Shu, C. -W. *Essentially non-oscillatory and weighted essentially non-oscillatory schemes for hyperbolic conservation laws*, Advanced numerical approximation of nonlinear hyperbolic equations (Cetraro, 1997), 325–432, Lecture Notes in Math., 1697, Fond. CIME/CIME Found. Subser., Springer, Berlin, 1998.

33. Shu, C. -W. and Osher, S. *Efficient implementation of essentially nonoscillatory shock-capturing schemes*, J. Comput. Phys. 77 (1988), no. 2, 439–471.

34. Turing, M. A. *The chemical basis of morphogenesis*, Philos. Trans. Roy. Soc. London Ser. B 237 (1952), no. 641, 37–72.

35. van Leer, B. *Towards the ultimate conservative difference scheme V. A second-order sequel to Godunov's method*, J. Comput. Phys. 32 (1979), no. 1, 101–136.

36. Vázquez, J. L. *The Porous Medium Equation: Mathematical Theory*, Oxford University Press, USA, 2007.

37. Witelski, T. P. *Segregation and mixing in degenerate diffusion in population dynamics*, J. Math. Biol. 35 (1997), no. 6, 695–712.

38. Zel'dovich, Y. B. and Kompaneetz, A. S. *Towards a theory of heat conduction with thermal conductivity depending on the temperature*, in: Collection of Papers Dedicated to 70th Birthday of Academician A.F. Ioffe, Izd. Akad. Nauk SSSR, Moscow, 1950, pp. 61–71.

39. Zhang, Q. and Wu, Z. -L. *Numerical simulation for porous medium equation by local discontinuous Galerkin finite element method*. J. Sci. Comput. 38 (2009), no. 2, 127–148.

روش‌های وزن‌دار غیرنوسانی برای معادلات با مشتقات جزئی چندبعدی غیرخطی سهموی تباهیده

روح‌اله عابدیان

دانشگاه تهران، پردیس دانشکده‌های فنی، دانشکده علوم مهندسی

دریافت مقاله ۲۹بهمن ۱۳۹۵، دریافت مقاله اصلاح شده ۱۷ اردیبهشت ۱۳۹۶، پذیرش مقاله ۲۱ تیر ۱۳۹۶

چکیده : در این مقاله، یک روش برای تقریب جواب‌های معادلات غیرخطی سهموی تباهیده که ممکن است دارای ناپیوستگی در جواب‌ها باشند را ارائه می شود. در حالت یک بعدی، همانند ایده روش گلرکین ناپیوسته موضعی، ابتدا معادله سهموی تباهیده به صورت یک سیستم غیرخطی مرتبه یک در نظرگرفته می‌شود و سپس این سیستم با استفاده از یک روش تفاضلات متناهی وزن‌دار غیرنوسانی برای معادلات قوانین پایستگی حل می‌گردد. این برای اولین بار است که محدود کننده مینمد همراه با ایده روش وزن‌دار غیرنوسانی برای معادلات سهموی تباهیده به‌کار گرفته می‌شود. همچنین ذکر این نکته ضروری است که دقت روش جدید در نواحی هموار از مرتبه پنج و در نواحی تکینگی از مرتبه دو می‌باشد. با استفاده از مسائل گوناگون چند بعدی، خواص دقت، استواری و وضوح بالا روش جدید نمایش داده می‌شود.

کلمات کلیدی : روش‌های وزن‌دار غیرنوسانی؛ روش تفاضلات متناهی؛ معادله چندبعدی غیرخطی سهموی تباهیده؛ معادله محیط متخلخل.